NASA Technical Memorandum 101455

The Oxidation of Ni-Rich Ni-Al Intermetallics

Joseph Doychak
Sverdrup Technology, Inc.
NASA Lewis Research Center Group
Cleveland, Ohio

and

James L. Smialek and Charles A. Barrett
National Aeronautics and Space Administration
Lewis Research Center
Cleveland, Ohio

Prepared for the
Workshop on the Oxidation of High-Temperature Intermetallics
sponsored by the Cleveland Chapter of ASM International and NASA Lewis Research Center in cooperation with Case Western Reserve University, The Metallurgical Society of AIME, and the Cleveland Chapter of TMS-AIME
Cleveland, Ohio, September 22-23, 1988

NASA

The Oxidation of Ni-Rich Ni-Al Intermetallics

Joseph Doychak
Sverdrup Technology, Inc.
NASA Lewis Research Center Group
Cleveland, Ohio 44135

and

James L. Smialek and Charles A. Barrett
National Aeronautics and Space Administration
Lewis Research Center
Cleveland, Ohio 44135

E-4438

Abstract

The oxidation of Ni-Al intermetallic alloys in the β-NiAl phase field and in the two phase β-NiAl/γ'-Ni_3Al phase field has been studied between 1000°C and 1400°C. The stoichiometric β-NiAl alloy doped with Zr was superior to other alloy compositions under cyclic and isothermal oxidation. The isothermal growth rates did not increase monotonically as the alloy Al content was decreased. The characteristically ridged α-Al_2O_3 scale morphology, consisting of cells of thin, textured oxide with thick ridges at cell boundaries, forms on oxidized β-NiAl alloys. The correlation of scale features with isothermal growth rates indicates a predominant grain boundary diffusion growth mechanism. The 1200°C cyclic oxidation resistance decreases near the lower Al end of the β-NiAl phase field.

Introduction

Aluminide intermetallics are being considered for use as matrix materials for high-temperature intermetallic matrix composites. Unlike most aluminides being considered, β-NiAl has excellent oxidation resistance as a result of the easy formation of protective Al_2O_3 scales. Although not as oxidation resistant as β-NiAl, γ'-Ni_3Al also readily forms protective Al_2O_3 scales during isothermal oxidation. There is an interest in using lower Al β-NiAl alloys and β/γ' alloys as high temperature structural materials because of possible increases in ductility relative to stoichiometric β-NiAl [1]. The isothermal oxidation of some alloys within this composition range has been performed [2], but the cyclic and isothermal oxidation of the more important rare-earth doped engineering Ni-Al alloys has not been studied systematically. Therefore, an understanding of the oxidation behavior of alloys ranging from the stoichiometric β-NiAl to γ'-Ni_3Al would be beneficial.

The current understanding of the oxidation behavior of both γ'-Ni_3Al and β-NiAl has been developed through many studies involving scale growth kinetics, scale morphologies and oxide adherence mechanisms [3-8]. For γ'-Ni_3Al, the oxidation mechanisms are similar to many alumina forming alloys. Upon exposure to the oxidizing environment, NiO, $NiAl_2O_4$, and Al_2O_3 form during a fast growth transient stage. The transient scales often consist of textured, fine-grained oxides. Eventually a healing α-Al_2O_3 layer forms beneath the transient scale and the scale growth rate decreases dramatically. Based on the columnar scale morphologies (Figure 1a) [3] and ^{18}O tracer measurements [9], the scale is believed to grow by inward oxygen grain boundary diffusion.

The oxidation mechanisms of β-NiAl differ from that of γ'-Ni_3Al. The transient stage of oxidation on β-NiAl results in the formation of predominantly metastable phases such as θ-Al_2O_3 and δ-Al_2O_3 [10]. The transient scale growth rates are comparable to the transient scales on γ'-Ni_3Al, because scale growth is controlled by outward cation diffusion. After an incubation period, the metastable Al_2O_3 phases transform to α-Al_2O_3, beginning at the gas/oxide surface and moving inward towards the scale/metal interface and radially along the scale [6]. This particular mechanism of Al_2O_3 formation results in a number of features in the scale which ultimately control the scale growth. The features are displayed in the schematic of a mature α-Al_2O_3 scale that would form on β-NiAl, shown in Figure 1b [6]. The transformation to α-Al_2O_3 involves an approximately 13% volume reduction. Therefore, radial tensile cracks develop in the scale which quickly heal by the formation of fine, equiaxed α-Al_2O_3 grains at the crack base. These regions appear to grow by inward oxygen grain boundary diffusion, because scale growth is observed only on the scale underside in these regions. The radial spreading of the transformed oxide results in a mosaic of textured, α-Al_2O_3 subgrains forming cells; each cell is the result of one nucleation event. The misorientations between subgrains are a minimum near the original nucleation point and are a maximum at the regions where adjacent cells meet. Ridges form along cell boundaries and along subgrain boundaries having relatively higher misorientations. The ridges form predominantly on the outside of the scale, and thus, are a result of outward cation diffusion. Therefore, overall scale growth results from both inward oxygen and outward Al diffusion along many different types of short-circuit paths.

Although much appears to be known about the oxidation mechanisms of γ'-Ni_3Al and β-NiAl, the current understanding can only be applied over a limited temperature range in which experimental data has provided evidence. Temperatures above 1300°C for β-NiAl and 1200°C for γ'-Ni_3Al have not been studied in depth because these temperatures are beyond the current usage temperature for the respective alloys. Cyclic oxidation data of these materials has been performed [11,12], but is sparse, even though this type of testing provides a more accurate depiction of usage conditions. Alloy compositions with respect to Al content and adherence-promoting elements have not been optimized. Therefore, more work needs to be done to provide a broader basis for the use of nickel aluminides in high temperature applications.

The purpose of the present program is twofold: a) to determine the effects of decreased Al contents on the isothermal and cyclic oxidation of β-NiAl and β-NiAl/γ'-Ni_3Al alloys, and b) to determine the upper temperature limits for usage based on degradation by

oxidation. Temperatures up to 1400°C at various alloy compositions between the stoichiometric β-NiAl and γ'-Ni_3Al phases are being studied in both cyclic and isothermal modes of oxidation. It is believed that a study of this nature should provide information involving limits on using these nickel aluminides for oxidation protection at high temperatures.

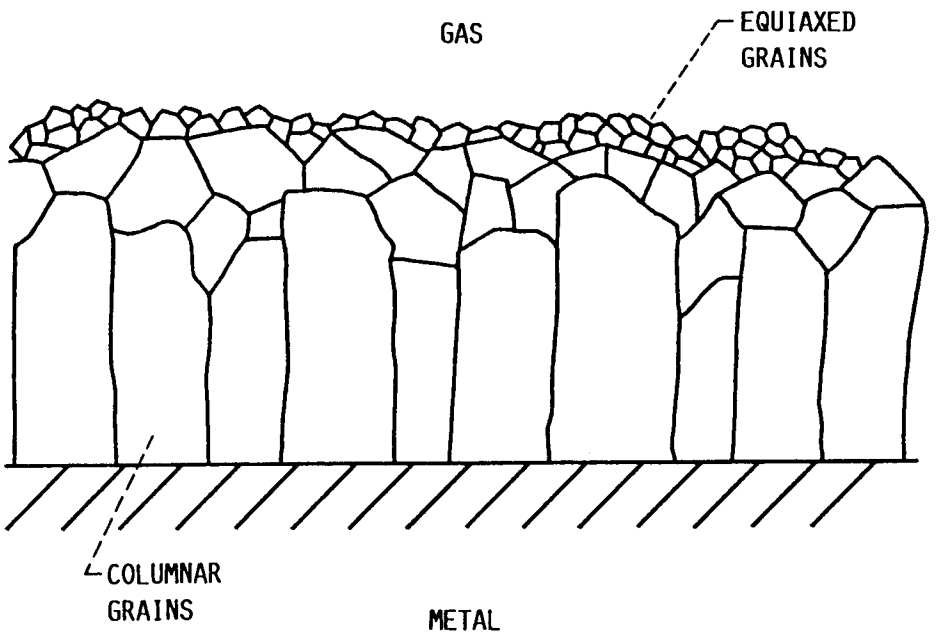

(a) COLUMNAR MORPHOLOGY.

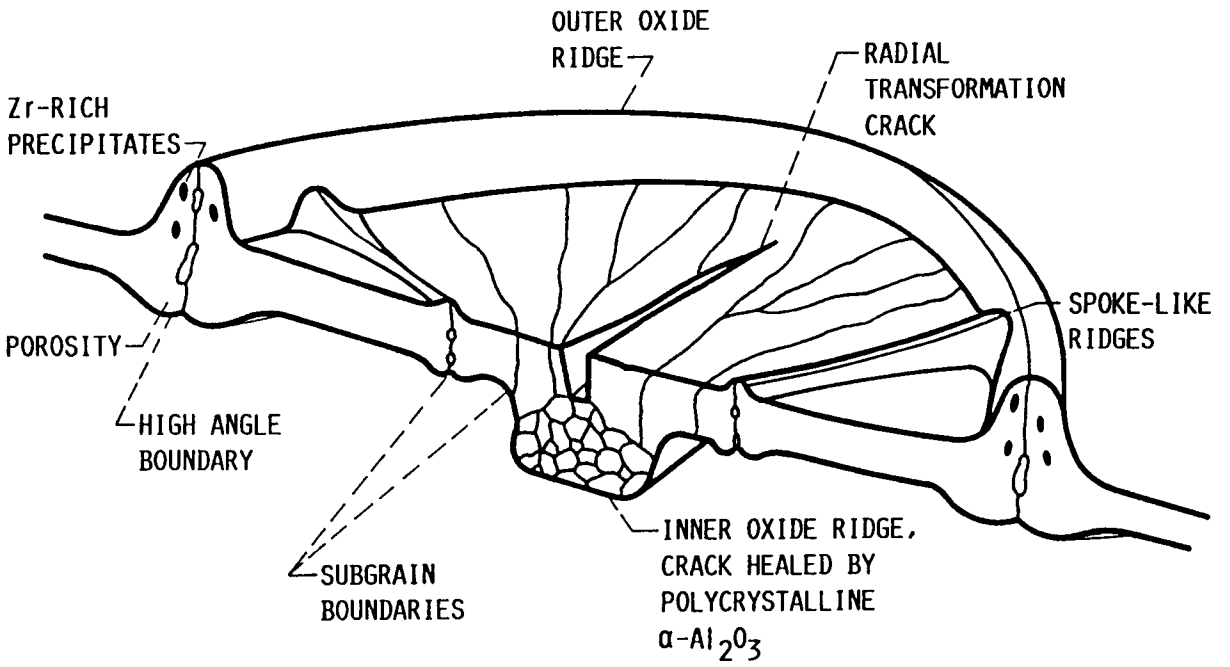

(b) RIDGED NETWORK MORPHOLOGY.

Figure 1. Schematics of α-Al_2O_3 morphologies that form on different alumina-forming alloys.

Experimental Procedures

Alloys were obtained by arc melting the prescribed amounts of high purity Ni, Al and Zr and drop casting in copper molds approximately 0.5 x 0.5 x 1.25 inches. The nominal and actual compositions (determined by various analytical techniques) of the twelve alloys are shown in Table I. Alloys will be referred to by their phase at room temperature, Al concentration and the absence or presence of 0.1 wt% Zr. For example, β50.2+ corresponds to β-NiAl having 50.2 at% Al with .04 at% (.1 wt%) Zr. The castings were spark machined into specimens approximately 1 x 1 x 0.1 cm. Specimens were abraded using consecutively finer grades of SiC paper, the final surface being 600 grit. Specimens were cleaned with soap water and rinsed in alcohol then acetone prior to oxidation.

Isothermal oxidation tests were performed using a Cahn 1000 thermogravimetric electrobalance apparatus. Cyclic testing was performed using a system combining an automatic pneumatic withdrawal apparatus with high temperature furnaces, which have been described elsewhere [12]. The data consisted of weight changes as a function of test time. Oxidation tests were performed at 100°C intervals between 1000°C and 1400°C in flowing oxygen (isothermal) and stagnant air (cyclic). Isothermal tests were performed for 100 hours. Cyclic tests were continued until significant amounts of non-protective oxides were formed.

Analysis of the specimens following oxidation treatments consisted of scanning electron microscopy (SEM), X-ray diffraction (XRD), optical microscopy and some transmission electron microscopy (TEM).

Table I. Nominal and Actual Alloy Compositions (at%)

Designations	Nominal	Actual
β50.2+	Ni-50.0Al-.05Zr	Ni-50.2Al-.04Zr
β49.4−	Ni-50.0Al	Ni-49.4Al
β46.8+	Ni-46.5Al-.05Zr	Ni-46.8Al-.05Zr
β43.9+	Ni-43.0Al-.05Zr	Ni-43.9Al-.04Zr
β39.9+	Ni-39.0Al-.05Zr	Ni-39.9Al-.04Zr
β37.5+	Ni-36.5Al-.05Zr	Ni-37.5Al-.04Zr
β/γ'35.5+	Ni-34.0Al-.05Zr	Ni-35.5Al-.04Zr
β/γ'33.2+	Ni-32.0Al-.05Zr	Ni-33.2Al-.04Zr
β/γ'31.1−	Ni-30.0Al	Ni-31.1Al
β/γ'30.6+	Ni-30.0Al-.05Zr	Ni-30.6Al-.04Zr
β/γ'29.0+	Ni-27.5Al-.05Zr	Ni-29.0Al-.04Zr
β/γ'26.8+	Ni-25.0Al-.05Zr	Ni-26.8Al-.04Zr

Results

Isothermal Oxidation

Oxidation Kinetics. An Arrhenius plot of the parabolic growth rates versus temperature are shown in Figure 2a, for the higher Al content alloys, and Figure 2b, for the lower Al content alloys. The parabolic growth rate constants, k_p (measured in $mg^2/cm^4/hr$), were determined using the steady-state portion of the kinetic curve rather than the combined transient and steady-state portions [13]. In most cases, the kinetic curves followed a parabolic rate law. However, an upward deviation, implying faster growth kinetics than parabolic, was observed for some lower Al content alloys, especially at the higher temperatures. In these cases, k_p values were estimated from the regions showing faster growth kinetics.

The data of Figure 2, in general, are within a band ranging from 0.5 to 2.5 orders of magnitude wide for the temperature range covered. The experimental scatter of each data point (determined by repeated tests) was negligible relative to the large differences in measured growth rate constants shown in Figure 2. Activation energies were determined using regression analysis from the oxidation kinetics at 1100°C and above for each individual alloy (Table II). There is no general trend of activation energy with alloy composition. The highest activation energy obtained was for the oxidation of β50.2+. All values are in the range of previously determined values for the oxidation of similar alloys [2,13]. The activation energies of alloys without Zr are much less than those of similar alloys with Zr.

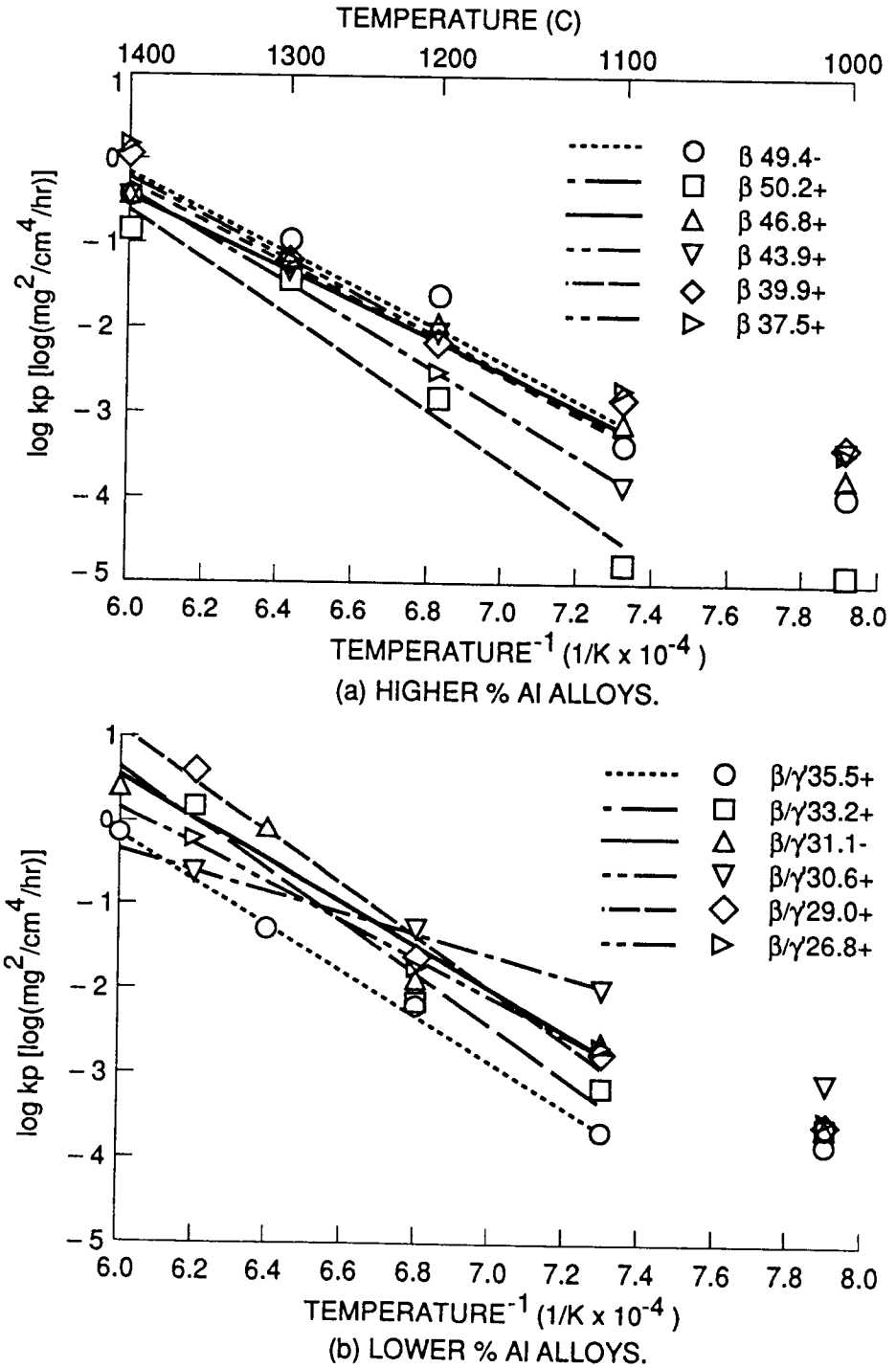

Figure 2. Arrhenius plots of parabolic growth rate constants as a function of temperature.

The large reduction in activation energy for alloys without Zr arises from increased k_p values at the lower temperatures. For example, at 1200°C in Figure 2a, β50.2+ had the slowest growth rate, whereas β49.4− had the highest growth rate. The same is true for the lower Al alloys in Figure 2b. The growth rate is generally higher for the alloys without Zr.

A major observation in Figure 2 is that the k_p values do not increase monotonically with decreasing alloy Al concentration. This point is shown more dramatically in Figure 3 which is a plot of k_p values versus Al concentration at each temperature for alloys with Zr additions. Although the endpoints of each curve suggest that the k_p values increase with decreasing alloy Al concentration, no continuous trend exists. Therefore, an exact correlation of alloy Al content with scale growth rate is improbable.

Table II. Activation Energies for Isothermal Oxidation (1100°C - 1400°C)

Alloy	Q (kcal/mole/deg)
β50.2+	60.8
β49.4−	43.9
β46.8+	42.1
β43.9+	50.5
β39.9+	43.7
β37.5+	44.8
β/γ'35.5+	52.4
β/γ'33.2+	52.9
β/γ'31.1−	23.9
β/γ'30.6+	50.0
β/γ'29.0+	60.3
β/γ'26.8+	43.9

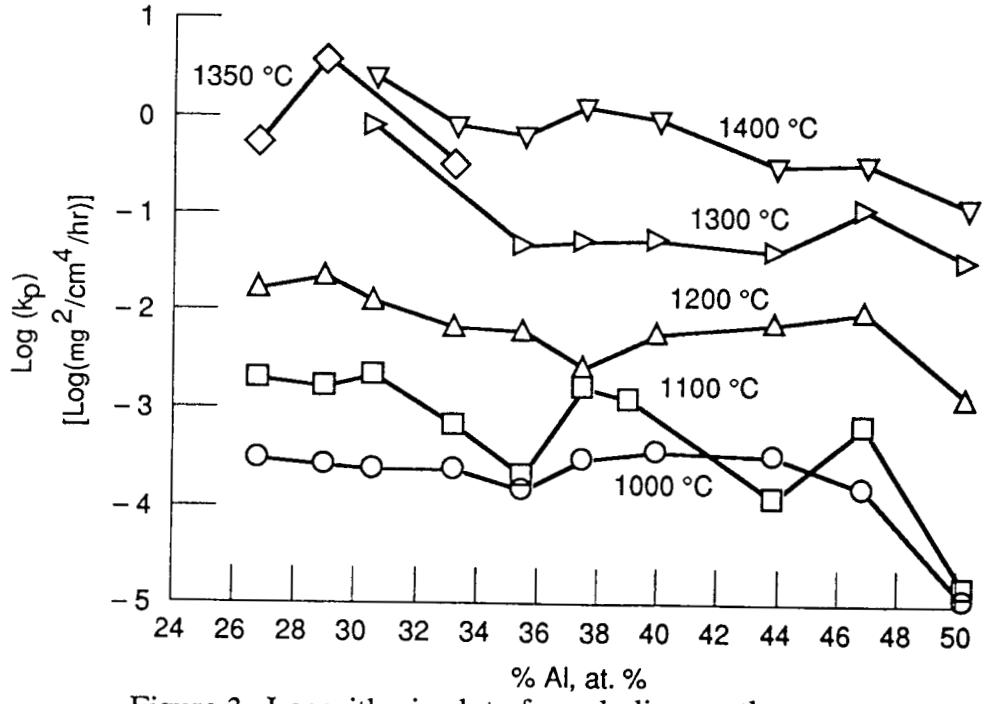

Figure 3. Logarithmic plot of parabolic growth rate constants as a function of aluminum content for the various oxidation temperatures.

Scale Morphologies. The scale surface morphologies after 100 hours of isothermal oxidation were studied using SEM. The scale morphologies on β50.2+ as a function of temperature are shown in Figure 4. The morphology that forms at 1000°C (Figure 4a) consists of needles or platelets of oxide throughout. These are remnant of the transient scales which tend to grow by outward cation diffusion [10,6]. However, a broad ridge and radial transformation cracks also evident indicate that the scale has transformed (or partially transformed) to α-Al_2O_3, and is beginning to form the ridge morphology as described earlier. At 1100°C (Figure 4b), distinct ridges have formed outlining large (10-20 μm diameter) cells. The scale surface within cells has smoothed by surface diffusion [6], but still shows remnants of the transient morphology. The morphology differs at 1200°C (Figure 4c) in that the spoke ridges are similar in character to ridges outlining cells. Individual cells can be delineated and are still quite large. At 1300°C (Figure 4d), distinct cells and ridges cannot be clearly defined, because the overall morphology is too coarse. Fine precipitates observable on the scale surface are rich in Zr. The scale morphology at 1400°C (Figure 4e) is extremely coarse and shows similar features as the 1300°C morphology.

Figure 5 is a series of SEM micrographs of scale morphologies formed on different alloys at 1200°C. Figure 5a is from a β50.2+ alloy, and is similar to Figure 4c. The morphology shown in Figure 5b is from the β43.9+ alloy. The cell sizes are smaller (≈ 2-5 μm) and the ridges are thicker. The scale morphology that formed on β37.5+ (Figure 5c) contains slightly larger cells (≈ 8-10 μm) and ridges having a similar thickness to those of the β50.2+ morphology. The scale is convoluted and contains linear cracks throughout which do not appear to be related to the transformation process, but most likely occur during specimen cooling. Figure 5d shows the morphology formed on β/γ'35.5+. The morphology is similar in all respects to the morphology that formed on β43.9+ (Figure 5b). The alloy is two-phase β/γ' at room temperature, but becomes strictly β-NiAl at 1200°C. No indications of the ridge network are observable in the microstructure that formed on β/γ'30.6+. Although the alloy microstructure is two-phase at 1200°C and consists of lathes of γ'-Ni_3Al amongst a β-NiAl matrix, the scale morphology is uniform throughout and is similar to scales that form on NiCrAlY alloys [14]. TEM investigations of the scale that formed after .05 hours at 1100°C on this alloy reveal a thicker oxide consisting of predominantly $NiAl_2O_4$ on the γ'-Ni_3Al phase, and a thinner oxide consisting of predominantly θ-Al_2O_3 on the β-NiAl phase (Figure 6).

The scale morphologies provide information regarding the scale growth mechanisms. For example, by comparing the cell sizes of the ridge network with the scale growth rates, as was done for oxidation at 1200°C shown in Figure 7, it is apparent that the larger the cell size the slower the growth rate. This indicates that scale growth occurs by predominantly boundary diffusion. A larger cell size implies less boundary area, and therefore, an overall smaller flux of diffusing species. This situation is similar to the effect of scale grain size on growth rates [15].

Similar arguments can be applied for the oxidation at 1000°C. Figures 8a through 8c show the scale morphologies formed on β50.2+, β43.9+, and β/γ'35.3+, respectively. The corresponding k_p values for oxidation on the respective alloys are 1.8×10^{-5}, 3.3×10^{-4}, and 1.5×10^{-4} $mg^2/cm^4/hr$. The largest cell size (Figure 8a) corresponds to the slowest growth rate. The smallest cell size (Figure 8b) corresponds to the fastest growth rate.

The k_p value at 1100°C for β50.2+ (with Zr) is 1.3×10^{-3} $mg^2/cm^4/hr$ whereas the k_p value for β49.4− (without Zr) is 2.2×10^{-2} $mg^2/cm^4/hr$ (Figure 2a). A decrease of over one order of magnitude occurred when as little as 0.1 wt% Zr was added to the alloy. This effect is observed in the scale morphologies that formed on these alloys shown in Figure 9. The morphology shown in Figure 9a is for β50.2+ oxidized at 1100°C and contains large cells and narrow ridges; the morphology corresponds to the slow growth rate. The morphology shown in Figure 9b is for β49.4− oxidized at 1100°C and contains small cells and very thick ridges; this morphology corresponds to a high growth rate. Whiskers of oxide are observed in the β49.4− scale whereas no whiskers are observed in the β50.2+ scale.

(a) 1000 ^{o}C.

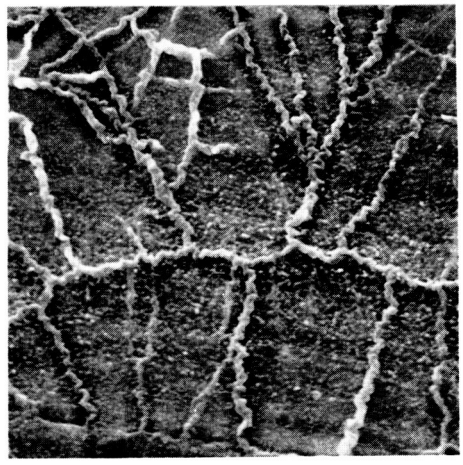

(b) 1100 ^{o}C.

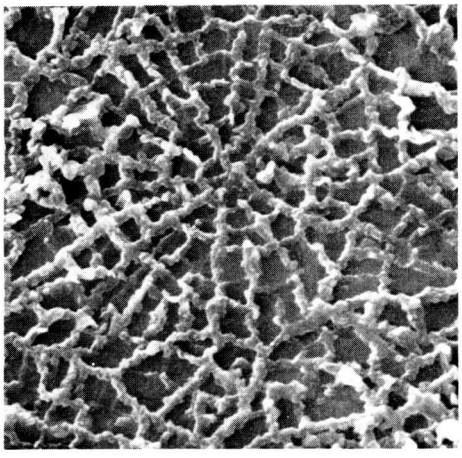

(c) 1200 ^{o}C.

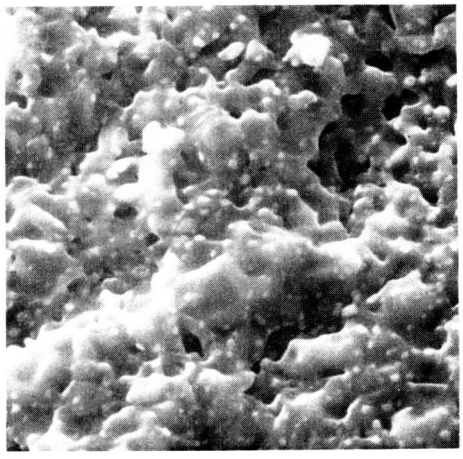

(d) 1300 ^{o}C.

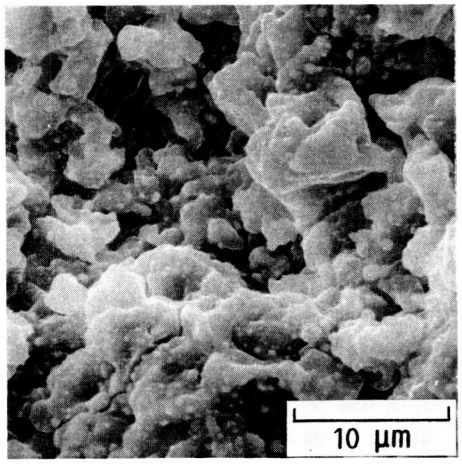

(e) 1400 ^{o}C.

Figure 4. SEM micrographs of scale surface morphologies that formed after oxidation a β50.2+ alloy for 100 hours.

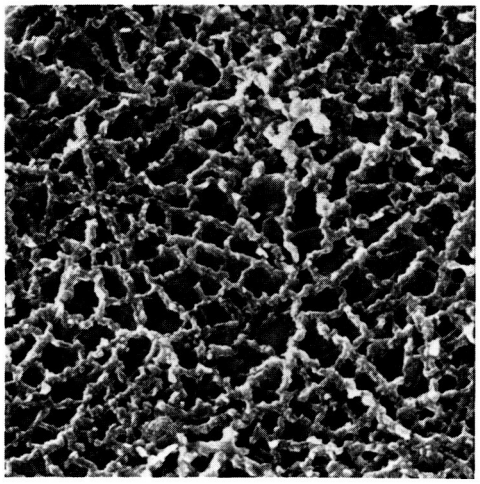

(a) β50.2+.

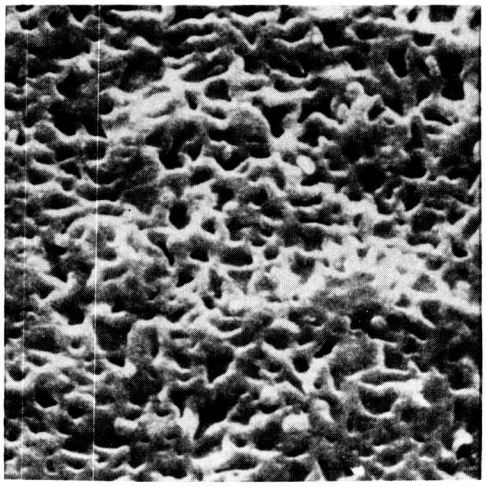

(b) β43.9+.

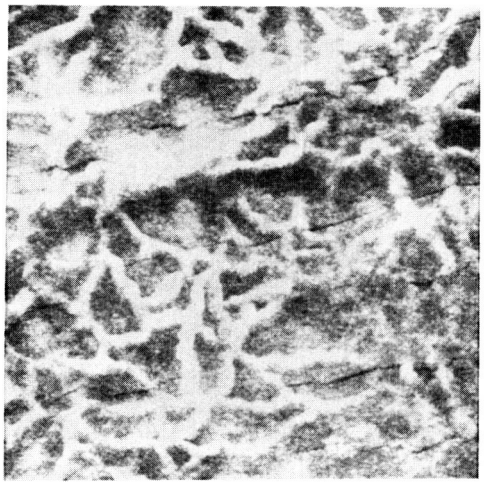

(c) β37.5+.

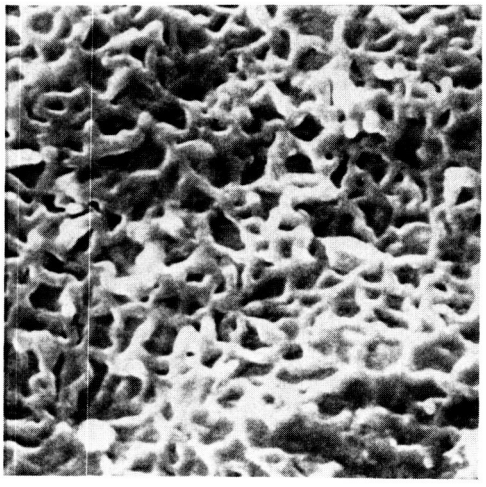

(d) β/γ'35.5+.

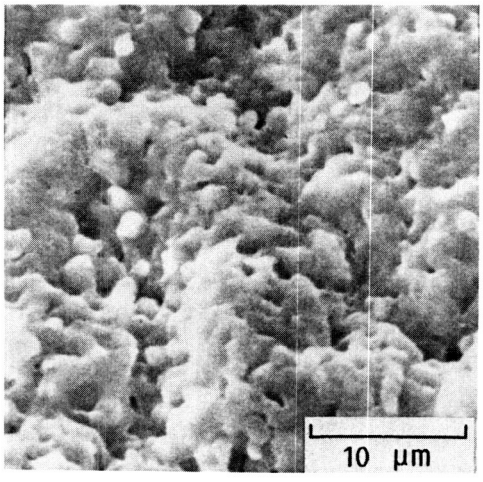

(e) β/γ'30.6+.

Figure 5. SEM micrographs of scale surface morphologies that formed after oxidation for 100 hours at 1200°C.

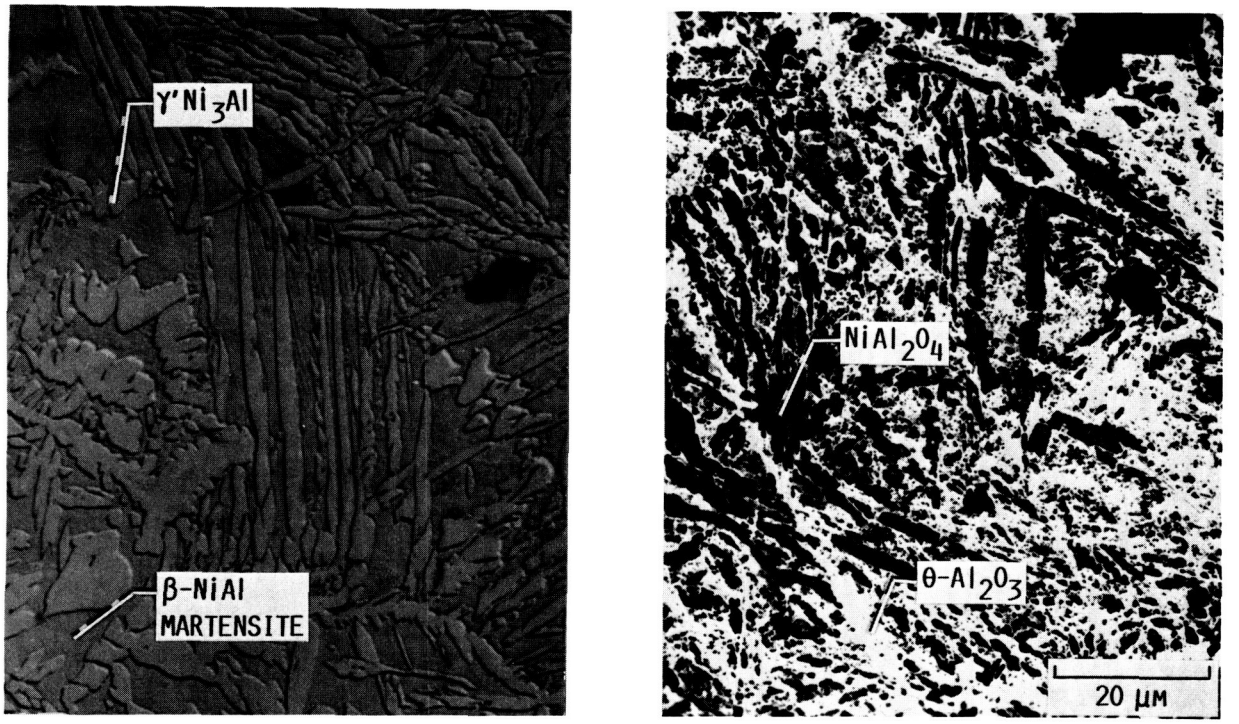

(a) ALLOY SUBSTRATE; OPTICAL. (b) OXIDE SCALE, TEM BF.

Figure 6. Micrographs of a β/γ'33.2+ alloy and corresponding oxide formed after 0.05 hr oxidation at 1100°C: a) optical micrograph showing γ'-Ni_3Al lathes amongst a β-NiAl matrix; b) TEM bright field micrograph showing θ-Al_2O_3 that formed over the β-NiAl matrix and $NiAl_2O_4$ that formed over the γ'-Ni_3Al lathes.

Cyclic Oxidation

Cyclic oxidation was performed at 1200°C. Thermal cycles consisted of one hour at temperature followed by an approximately 20 minute cooldown to slightly above ambient temperature. The results after 200 cycles are shown in Figure 10 which is a plot of weight change per unit area versus Al content. The results indicate that below approximately 40 at% Al, the cyclic oxidation resistance degrades rapidly. XRD analysis of the spalled scales and the scales remaining on the alloy surface indicate that the sudden drop in weight change corresponds to an increase in the presence of a less protective scale consisting of predominantly $NiAl_2O_4$. The upturn in the weight change curve corresponds to the presence of NiO. This indicates that NiO formation overcompensates for the weight loss which occurs by oxide scale spallation. The sudden upturn in weight change occurs at an Al concentration which is within the two-phase β/γ' region of the phase diagram at 1200°C, directly adjacent to the β-NiAl phase field.

The obvious outlyer in the data shown in Figure 10 occurs at an Al concentration of 35.5 at%. This alloy is within the β-NiAl phase field at 1200°C but is within the two-phase β/γ' phase field at temperatures less than 1200°C. No scale spallation was observed on this alloy. Also, the volume of the specimen increased with repeated testing. The alloy microstructure indicates that as the specimen is cooled, γ'-Ni_3Al precipitates on alloy grain boundaries. During further cooling, the β-NiAl matrix undergoes a martensitic transformation which involves a volume expansion. It is believed that the volume expansion counteracts the stress related to thermal expansion mismatch between the scale and alloy which would ultimately result in scale spallation. This effective stress relief minimizes spalling such that the cyclic weight changes approximate those measured after isothermal growth.

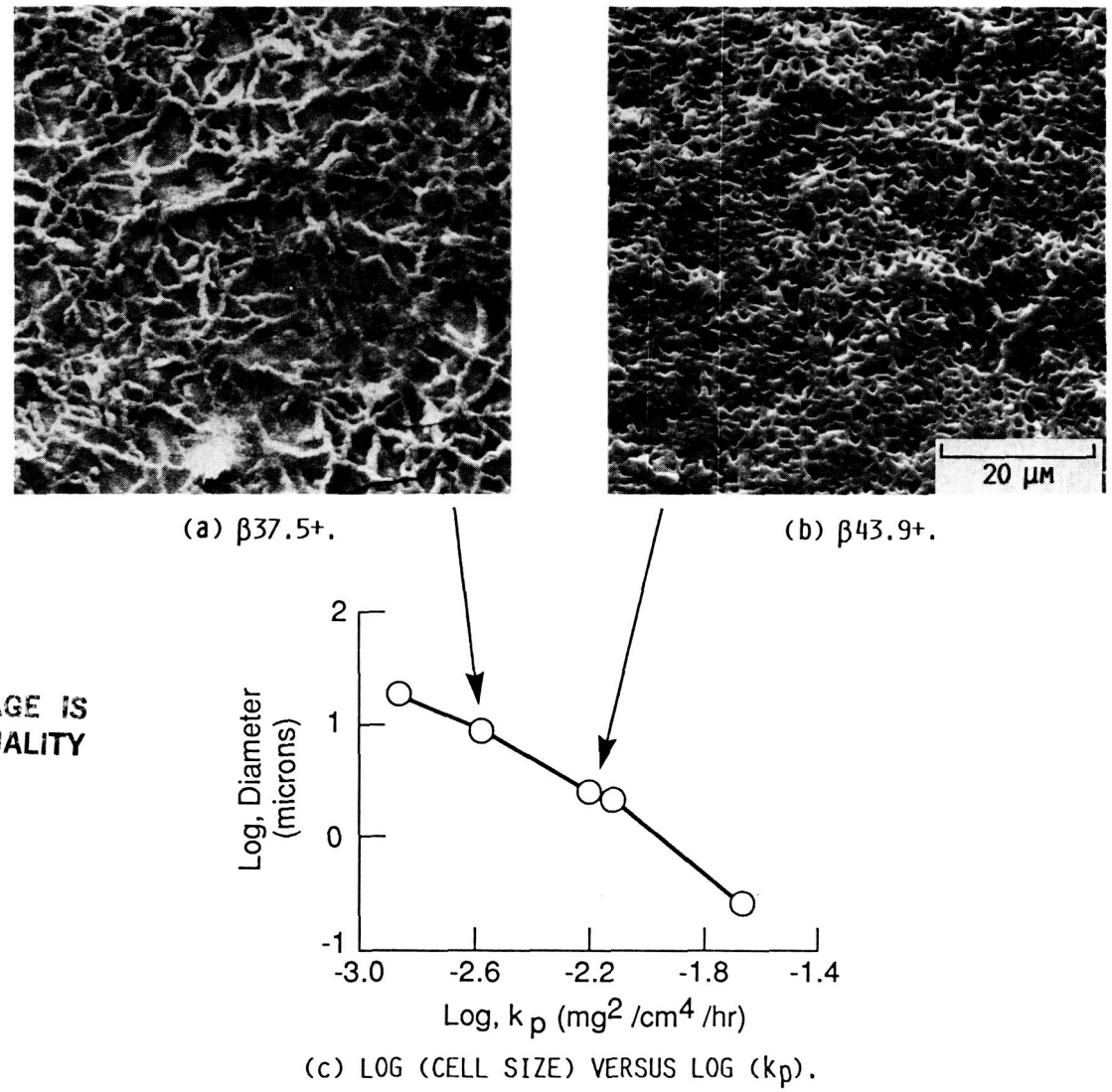

Figure 7. SEM micrographs of scale surface morphologies after oxidation for 100 hours at 1200°C and corresponding plot of cell size as a function of scale growth rate constant.

Discussion

The isothermal oxidation of Ni-Al alloys in the β-NiAl and two-phase β/γ' phase fields resulted in parabolic scale growth rate constants that are not directly related to alloy Al concentration. The slowest growth rate at temperatures between 1100°C to 1400°C was for β50.2+, a stoichiometric β-NiAl alloy containing .04 at% Zr. The fastest growth rate at these temperatures was not always for the lowest Al-containing alloy, β/γ'26.5+. However, for the β-NiAl alloys, a direct relationship existed between scale growth rates and scale morphologies. All β-NiAl alloys resulted in oxide scales having the ridged morphology. The smaller the cell sizes and the thicker the ridges, the faster were the scale growth rates. This implies a boundary diffusion mechanism for scale growth.

Alloy Zr concentration was found to have a large effect on scale growth rates and morphologies. For β-NiAl without Zr, scale growth rates sometimes were an order of magnitude or more greater than for β-NiAl with Zr. The ridge morphology on β-NiAl without Zr consisted of smaller cells and thicker ridges than the scale which formed on β-NiAl with Zr. In addition, whiskers were observed in the scale formed on β-NiAl without Zr. Thicker ridges and the presence of whiskers imply an outward Al diffusion mechanism. Zr additions appear to suppress the extent of Al outward diffusion as suggested previously [7].

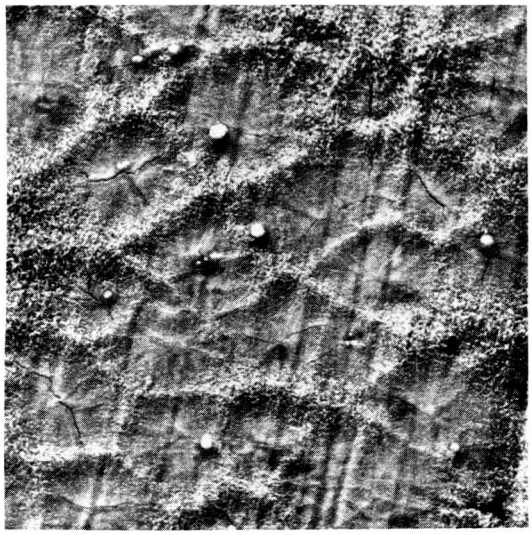

(a) β50.2+, $k_p = 1.18 \times 10^{-5}$ $MG^2/CM^4/HR$.

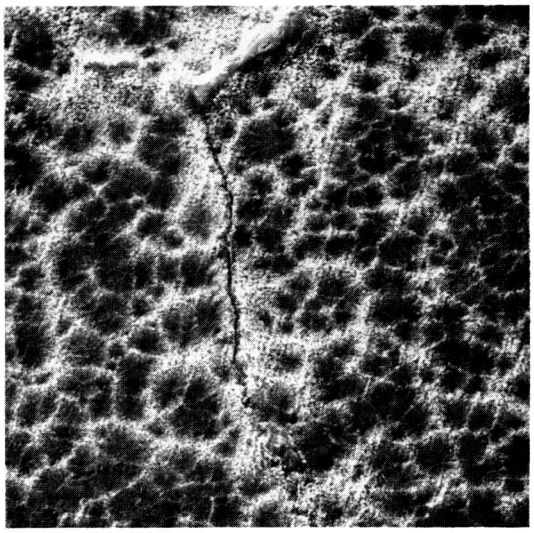

(b) β43.9+, $k_p = 3.28 \times 10^{-4}$ $MG^2/CM^4/HR$.

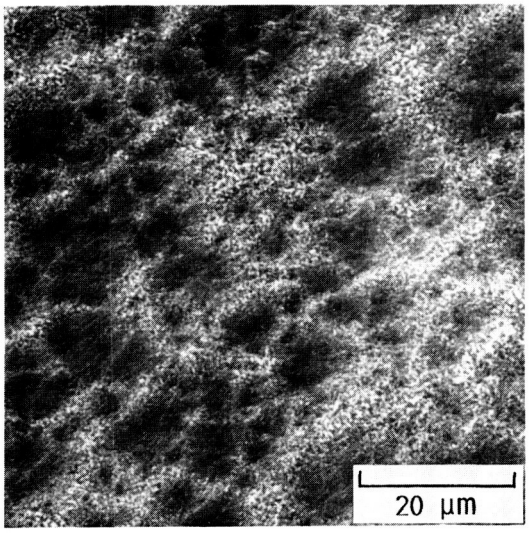

(c) β/γ'35.5+, $k_p = 1.51 \times 10^{-4}$ $MG^2/CM^4/HR$.

Figure 8. SEM micrographs of scale surface morphologies after oxidation for 100 hours at 1000°C and corresponding scale growth rate constants.

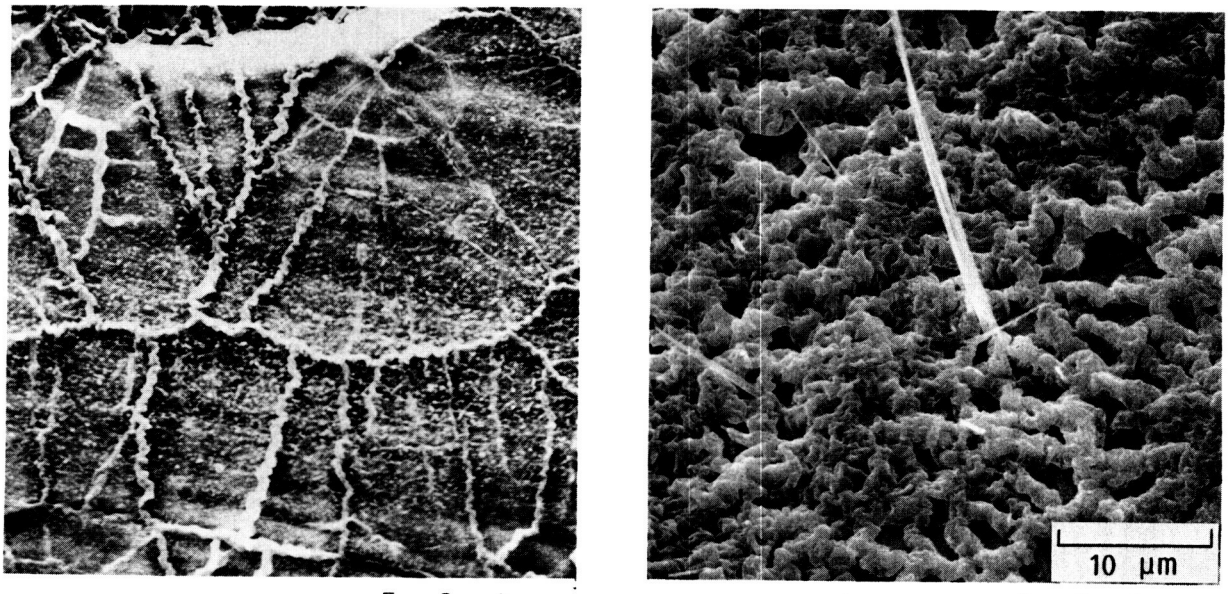

(a) β50.2+, k_p = 1.34x10^{-5} MG^2/CM^4/HR. (b) β49.5-, k_p = 2.2x10^{-2} MG^2/CM^4/HR.

Figure 9. SEM micrographs of scale surface morphologies and corresponding growth rate constants after oxidation for 100 hours at 1100°C.

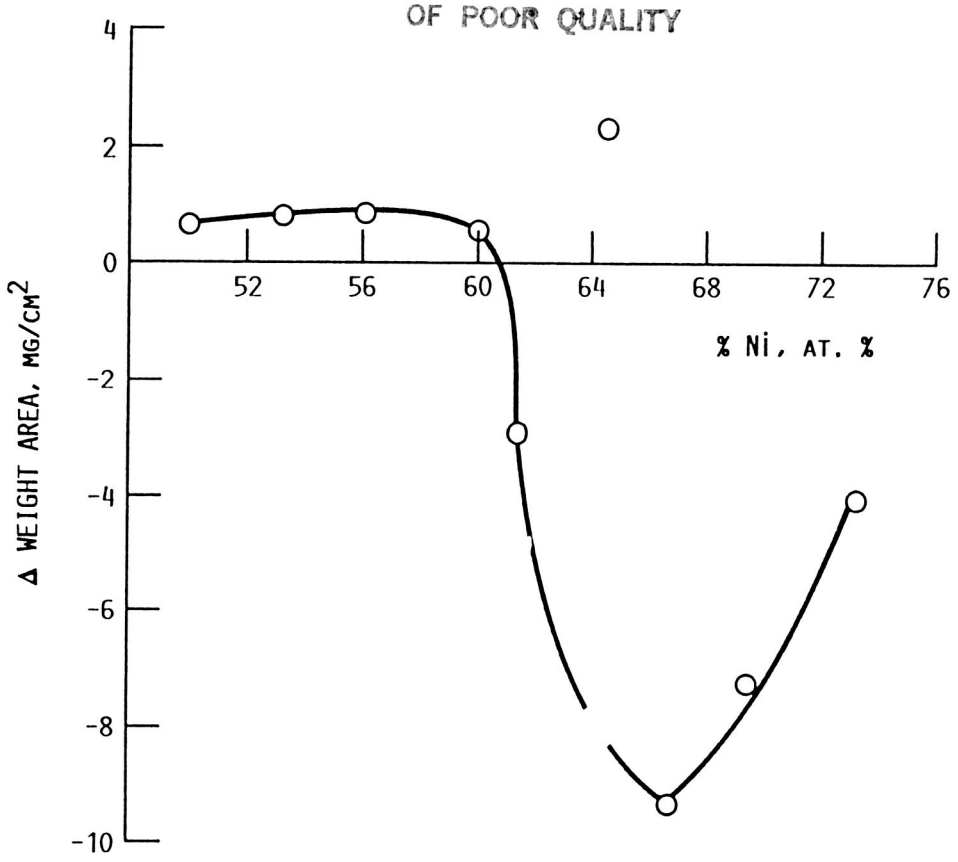

Figure 10. Specific weight change plot as a function of alloy aluminum content for cyclic oxidation at 1200°C for 200, 1-hour cycles.

Smaller cell sizes would suggest a faster nucleation of the transformation to α-Al_2O_3. Zr was found to drastically suppress the transformation in bulk Al_2O_3 [16], and could be responsible for fewer α-Al_2O_3 nuclei resulting in larger cell sizes. Although the ridge network, the presence of which would definitively suggest outward Al diffusion, was not observed on the two-phase β/γ' alloys, the growth rates were still reduced with Zr additions suggesting that Zr reduces aluminum and/or oxygen diffusion within the scale.

The cyclic oxidation of Ni-Al alloys doped with Zr in the β-NiAl and two-phase β/γ' phase fields resulted in a sharp drop in the weight change per unit area at approximately 40 at% Al after 200 1-hour cycles at 1200°C. Coupled with the onset of $NiAl_2O_4$ formation, this implies that an insufficient amount of Al is present at the scale/metal interface to sustain the formation of a protective Al_2O_3 scale. Therefore, specimens originally containing less than 40 at% Al have exceeded their useful life as an oxidation resistant material under these experimental conditions. Because diffusion within the alloy is a limiting factor, specimen thickness, temperature, the number of cycles and cycle time will all play a role in determining the point at which a protective Al_2O_3 scale can no longer form [17,18].

Summary of Results

1) The 1200°C cyclic oxidation resistance of β-NiAl + Zr after 200 1-hour cycles is degraded for specimens containing less than 40 at% Al.

2) The isothermal growth rates of Ni-Al alloys doped with Zr in the β-NiAl and two-phase β/γ' phase fields do not have a direct relationship with alloy Al concentration. However, there is a direct relationship between scale morphology and scale growth rates for β-NiAl alloys.

3) The ridge morphology of oxide scales forms throughout the β-NiAl phase field.

4) Additions of Zr reduce the scale growth rates of alloys in the β-NiAl and two-phase β/γ' phase fields. Additions of Zr to β-NiAl alloys tend to eliminate whisker formation and reduce the thickness of scale ridges, suggesting a suppression of outward Al diffusion through the scale.

Conclusions

1) The effect of reduced Al contents on the isothermal oxidation of β-NiAl + Zr up to 100 hours is to increase the growth rate of the scale relative to the stoichiometric alloy in a non-monotonic fashion. Surface features of the scale morphology change correspondingly with scale growth rate.

2) The upper temperature limit for Zr-doped Ni-Al alloys with less than approximately 40 at% Al is below 1200°C, based on a 200, 1-hour cyclic oxidation criterion of positive weight change. Cyclic oxidation studies at higher temperatures are required to set the temperature limits for NiAl + Zr alloys having greater than approximately 40 at% Al.

Acknowledgements

The authors wish to thank D.L. Humphrey for providing support to the oxidation experiments. This work was funded under the HITEMP program at NASA Lewis Research Center.

NASA
National Aeronautics and Space Administration

Report Documentation Page

1. Report No.	2. Government Accession No.	3. Recipient's Catalog No.
NASA TM-101455		

4. Title and Subtitle	5. Report Date
The Oxidation of Ni-Rich Ni-Al Intermetallics	6. Performing Organization Code

7. Author(s)	8. Performing Organization Report No.
Joseph Doychak, James L. Smialek, and Charles A. Barrett	E-4438
	10. Work Unit No. 510-01-01

9. Performing Organization Name and Address	11. Contract or Grant No.
National Aeronautics and Space Administration Lewis Research Center Cleveland, Ohio 44135-3191	13. Type of Report and Period Covered Technical Memorandum

12. Sponsoring Agency Name and Address	14. Sponsoring Agency Code
National Aeronautics and Space Administration Washington, D.C. 20546-0001	

15. Supplementary Notes

Prepared for the Workshop on the Oxidation of High-Temperature Intermetallics sponsored by the Cleveland Chapter of ASM International and NASA Lewis Research Center in cooperation with Case Western Reserve University, The Metallurgical Society of AIME, and the Cleveland Chapter of TMS-AIME, Cleveland, Ohio, September 22-23, 1988. Joseph Doychak, Sverdrup Technology, Inc., NASA Lewis Research Center Group, Cleveland, Ohio; James Smialek and Charles Barrett, NASA Lewis Research Center.

16. Abstract

The oxidation of Ni-Al intermetallic alloys in the β-NiAl phase field and in the two phase β-NiAl/γ'-Ni_3Al phase field has been studied between 1000 °C and 1400 °C. The stoichiometric β-NiAl alloy doped with Zr was superior to other alloy compositions under cyclic and isothermal oxidation. The isothermal growth rates did not increase monotonically as the alloy Al content was decreased. The characteristically ridged α-Al_2O_3 scale morphology, consisting of cells of thin, textured oxide with thick ridges at cell boundaries, forms on oxidized β-NiAl alloys. The correlation of scale features with isothermal growth rates indicates a predominant grain boundary diffusion growth mechanism. The 1200 °C cyclic oxidation resistance decreases near the lower Al end of the β-NiAl phase field.

17. Key Words (Suggested by Author(s))	18. Distribution Statement
Oxidation; Aluminides; Intermetallics; Ni-Al	Unclassified – Unlimited Subject Category 26

19. Security Classif. (of this report)	20. Security Classif. (of this page)	21. No of pages	22. Price*
Unclassified	Unclassified	16	A03

NASA FORM 1626 OCT 86

*For sale by the National Technical Information Service, Springfield, Virginia 22161

References

1. K. C. Russell and J. W. Edington, "Precipitation Behaviour and Mechanical Properties of a Nickel-36 at% Aluminium Alloy," Metal Science Journal, 6(1972), 20-24.

2. F. S. Pettit, "Oxidation Mechanisms for Nickel-Aluminum Alloys at Temperatures Between 900° and 1300°C," Trans. Met. Soc. AIME, 239(1967), 1296-1305.

3. J. D. Kuenzly, D. L. Douglass, "The Oxidation Mechanism of Ni_3Al Containing Yttrium," Oxid. Met., 8(1974), 139-178.

4. S. Taniguchi and T. Shibata, "Cyclic Oxidation Behavior of Ni_3Al-0.1B Base Alloys Containing a Ti, Zr, or Hf Addition," Oxid. Met., 25(1986), 201-215.

5. J. L. Smialek, "Oxide Morphology and Spalling Model for NiAl," Met. Trans. A, 9A(1978), 309-320.

6. J. Doychak, "The Evolution and Growth of Al_2O_3 Scales on β- NiAl" (Ph.D. thesis, Case Western Reserve University, 1986).

7. J. Jedlinski and S. Mrowec, "The Influence of Implanted Yttrium on the Oxidation Behaviour of β-NiAl," Materials Science and Engineering, 87(1987), 281-287.

8. H. M. Hindam and W. W. Smeltzer, "Growth and Microstructure of α-Al_2O_3 on β-NiAl," J. Electrochem. Soc., 127(1980), 1630- 1635.

9. K. P. R. Reddy, J. L. Smialek, and A. R. Cooper, "^{18}O Tracer Studies of Al_2O_3 Scale Formation on NiCrAl Alloys," Oxid. Met., 17(1982), 429-449.

10. J. Doychak, J. L. Smialek, and T. E. Mitchell, "Transient Oxidation of Single Crystal β-NiAl," Met. Trans., in press.

11. C. A. Barrett, "The Effect of 0.1 Atomic Percent Zirconium Level on the Cyclic Oxidation Resistance of β-NiAl," Oxid. Met., in press.

12. C. E. Lowell and G. J. Santoro, "The 1200°C Cyclic Oxidation Behavior of two Nickel-Aluminum Alloys (Ni_3Al and NiAl) With Additions of Chromium, Silicon, and Titanium," NASA TN D- 6838, 1972.

13. G. C. Rybicki and J. L. Smialek, "Effect of the θ to α-Al_2O_3 Transformation on the Oxidation Behavior of β-NiAl+Zr," Oxid. Met., in press.

14. C. S. Giggens and F. S. Pettit, "Oxide Scale Adherence Mechanisms and the Effects of Yttrium, Oxide Particles and Externally Applied Loads on the Oxidation of NiCrAl and CoCrAl Alloys" (Report ARL 75-0234, Aerospace Research Laboratories, 1975).

15. J. L. Smialek and R. Gibala, "Diffusion Processes in Al_2O_3 Scales: Void Growth, Grain Growth, and Scale Growth," High Temperature Corrosion, ed. R. A. Rapp (Houston, TX: National Association of Corrsion Engineers, 1981), 274-283.

16. P. Burtin et al., "Influence of Surface Area and Additives on the Thermal Stability of Transition Alumina Catalyst Supports. I: Kinetic Data," Applied Catalysis, 34(1987), 225-238.

17. J. L. Smialek and C. E. Lowell, "Effects of Diffusion on Aluminum Depletion and Degradation of NiAl Coatings," J. Electrochem. Soc., 121(1974), 800-805.

18. J. A. Nesbitt and R. W. Heckel, "Diffusional Transport during the Cyclic Oxidation of γ + β, Ni-Cr-Al(Y,Zr) Alloys," Oxid. Met., 29(1988), 75-102.